Applied Mathematical Sciences, Vol. 15, 2021, no. 6, 283 - 295
HIKARI Ltd, www.m-hikari.com
https://doi.org/10.12988/ams.2021.914486

Velocity Profile for Magnetohydrodynamic Flow in Straight Horizontal Elliptical Pipe

David Kweyu, A. Wanyama Manyonge

Department of Pure and Applied Mathematics
Maseno University, Kenya

K. Jacob Bitok

Department of Mathematics and Computer Science
University of Eldoret, Kenya

Abstract

Velocity profile for Magnetohydrodynamic (MHD) fluid flow in a straight long pipe with elliptical cross section has been investigated. Governing equations are partial differential equations comprising Ohm's law of electromagnetism, θ- component of Navier-Stokes equation, equation of continuity and cross section of the pipe. Navier-Stokes equation is converted into ordinary differential equation utilizing similarity transformation and solved numerically embracing Finite Element Method (FEM). Results are presented in form of tables and graphs and disclose that: When Hartmann number is increased, velocity of the fluid decreases at the centre of the pipe. Raising gravitational force, Reynolds number and half major axis distance, leads to upsurge in fluid velocity at the centre of pipe, though, the surge is little for the last case. Velocity declines towards the periphery of the pipe to zero in all the four cases.

Mathematics Subject Classification: 35Q05

Keywords: Non-dimensionalisation, Finite Element Method, Mathematica

1 Introduction

MHD flow through pipes has many applications in many fields like MHD generators, cooling system with liquid metals, astrophysics etc [1]. Skouras *et.al* [3] obtained a numerical solution for time dependent MHD equations for channels of rectangular, circular and elliptical cross sections. They used Local Meshless Point Collocation (LMPC) method and plotted velocity and induced magnetic field for high values of Hartmann numbers i.e $Ha \leq 10^5$. Finite Difference Method solution for convection diffusion equations (MHD) flow was obtained by Prasanna and Ganesh [5]. They presented solutions for ducts of different cross sections namely square, rectangle, triangle, circle, ellipse, sector and annulus under steady state conditions. Graphs plotted showed that for all the cross sections, the velocity profile was flat in the core region.

2 Mathematical Formulation

MHD flow equations comprises Ohm's law of electromagnetism, θ-component of Navier-Stokes equation, the equation of continuity and cross section of pipe. A MHD fluid flow in a straight horizontal pipe of sufficient length and of elliptical cross-section in the x-y plane is considered. The fluid flows in the z direction through the pipe due to Lorentz and gravitational forces. An applied magnetic field with an intensity $\mathbf{B}$ is parallel to the y-direction. The domain, Ω, is the elliptical cross section of the pipe. The boundary, Γ, is the inside of the cross section of the pipe.

2.1 Assumptions

i. The flow is steady and velocity of fluid is $\mathbf{u} = \{u_r,\, u_\theta,\, 0\}$, where u_r and u_θ are fluid velocities in r and θ directions respectively.

ii. Directed magnetic field is $\mathbf{B} = \{B, 0, 0\}$ for θ-component, B is the component of incident magnetic field $\mathbf{B}$.

iii. Lorentz force in the θ-component is $f_\theta = \sigma B^2 u_\theta$, where σ is electrical conductivity.

iv. Gravitational forces, $\rho\mathbf{g}$, exist while pressure fields, p are negligible, $\mathbf{g}$ and ρ are gravitational field strength and fluid density respectively.

2.2 Governing Equations

Elliptical cross section of pipe is shown in figure 1. r is given by : $r^2 = \frac{a^2b^2}{a^2\sin^2\theta + b^2\cos^2\theta}$, where a and b are half of the ellipse's major and minor axes respectively.

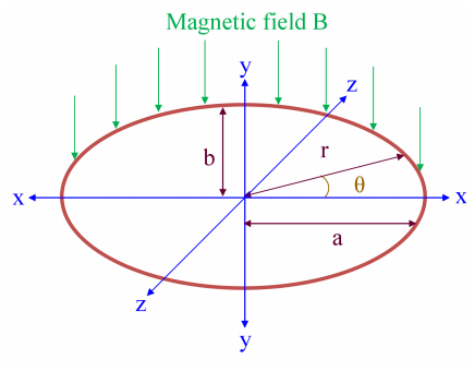

Figure 1: Elliptical cross section of pipe

Equation of continuity is given by :$\frac{1}{r}\frac{\partial}{\partial r}(ru_r) + \frac{1}{r}\frac{\partial}{\partial \theta}(u_\theta) = 0$
θ-component of Navier-Stokes equation is given as:

$$\rho\left(u_r\frac{\partial u_\theta}{\partial r} + \frac{u_\theta}{r}\frac{\partial u_\theta}{\partial \theta} + \frac{u_\theta u_r}{r}\right)$$
$$= \mu\left[\frac{1}{r}\frac{\partial}{\partial r}\left(r\frac{\partial u_\theta}{\partial r}\right) + \frac{1}{r^2}\frac{\partial^2 u_\theta}{\partial \theta^2} + \frac{2}{r^2}\frac{\partial u_r}{\partial \theta} - \frac{u_\theta}{r^2}\right] + f_\theta + \rho g_\theta \tag{1}$$

Ohms law of electromagnetism is given by:$\mathcal{J} = \sigma(\mathbf{E} + \mathbf{u} \times \mathbf{B})$, where $\mathcal{J}$ is electric current density and $\mathbf{E}$ is electric field respectively.

2.2.1 Non-dimensionalisation of Navier-Stokes equation

To non-dimensionalise equation (1), the following non-dimensional parameters [4] are engaged: $r = r^\star R, \theta = \theta^\star, u_r = u_r^\star U_0, u_\theta = u_\theta^\star U_0$, Reynolds number, $Re = \frac{RU_0}{\nu}$, kinematic viscosity, $\nu = \frac{\mu}{\rho}$, Hartmann number, $Ha = BR\left(\frac{\sigma}{\mu}\right)^{\frac{1}{2}}$ and Stuart number, $N = \frac{Ha^2}{Re}$, where U_0 and R are a characteristic velocity and a characteristic length from the centre of ellipse and μ is dynamic viscosity. Quantities with superscript stars are dimensionless quantities. From equation (1); $u_r\frac{\partial u_\theta}{\partial r} = \frac{U_0^2}{R}u_r^\star\frac{\partial u_\theta^\star}{\partial r^\star}$. Similarly, expressions for other terms in equation (1) are worked out, substituted in equation (1) together with $f_\theta = \sigma B^2 u_\theta$ and multiplying through by $\frac{R}{U_0^2\rho}$. Neglecting $\star$'s and letting $\frac{R}{U_0^2}g_\theta = \lambda_\theta$, gravitational force in the $\theta-$ component, equation (1) metamorphoses to

$$u_r\frac{\partial u_\theta}{\partial r} + \frac{u_\theta}{r}\frac{\partial u_\theta}{\partial \theta} + \frac{u_\theta u_r}{r} =$$
$$\frac{1}{Re}\left[\frac{1}{r}\frac{\partial u_\theta}{\partial r} + \frac{\partial^2 u_\theta}{\partial r^2} + \frac{1}{r^2}\frac{\partial^2 u_\theta}{\partial \theta^2} + \frac{2}{r^2}\frac{\partial u_r}{\partial \theta} - \frac{u_\theta}{r^2}\right] + Nu_\theta + \lambda_\theta \tag{2}$$

2.2.2 Navier-Stokes equation in terms of stream function

Given that $u_r = \frac{1}{r}\frac{\partial\psi}{\partial\theta}$ and $u_\theta = -\frac{\partial\psi}{\partial r}$, then for the first term in equation (2); $u_r\frac{\partial u_\theta}{\partial r} = -\frac{1}{r}\frac{\partial\psi}{\partial\theta}\frac{\partial^2\psi}{\partial r^2}$. Using the same method, the rest of the terms are written and set in equation (2), which delivers

$$\frac{\partial\psi}{\partial r}\frac{\partial^2\psi}{\partial r\partial\theta} - \frac{\partial\psi}{\partial\theta}\frac{\partial^2\psi}{\partial r^2} - \frac{1}{r}\frac{\partial\psi}{\partial\theta}\frac{\partial\psi}{\partial r} =$$

$$\frac{1}{Re}\left[\frac{1}{r}\frac{\partial\psi}{\partial r} + \frac{2}{r^2}\frac{\partial^2\psi}{\partial\theta^2} - \frac{1}{r}\frac{\partial^3\psi}{\partial\theta^2\partial r} - r\frac{\partial^3\psi}{\partial r^3} - \frac{\partial^2\psi}{\partial r^2}\right] - Nr\frac{\partial\psi}{\partial r} + \lambda_\theta \qquad (3)$$

boundary conditions:$\frac{1}{r}\frac{\partial\psi}{\partial\theta} = -\frac{\partial\psi}{\partial r} = 0$ on Γ

3 Numerical Solution of the Problem

3.1 Similarity Transformation

Equation (3) is converted into an ordinary differential equation by using similarity transformation, Abbott *et.al* [2]. The similarity transformation used is $\eta = \epsilon^{r^n\theta^n}$ such that $\psi = \epsilon^{r^n\theta^n}f(\epsilon^{r^n\theta^n})$, where n is an integer and ϵ is the base of natural logarithm. Considering the case when $n = -1$ for simplicity: since $\psi = \epsilon^{r^{-1}\theta^{-1}}f(\epsilon^{r^{-1}\theta^{-1}})$ then $\frac{\partial\psi}{\partial r} = -r^{-2}\theta^{-1}\epsilon^{r^{-1}\theta^{-1}}f(\epsilon^{r^{-1}\theta^{-1}}) - r^{-2}\theta^{-1}\epsilon^{2r^{-1}\theta^{-1}}f'(\epsilon^{r^{-1}\theta^{-1}})$. The procedure is repeated for other terms in equation (3), their products found and then placed in equation (3). Upon considering only terms whose coefficients are $r^{-1}\theta^{-1}$ or having their powers multiples of $r^{-1}\theta^{-1}$ and since $\eta = \epsilon^{r^{-1}\theta^{-1}}$, equation (3) becomes

$$\eta^4 log\eta^5 f'''(\eta) + 6\eta^3 log\eta^4 f''(\eta) + 6\eta^3 log\eta^5 f''(\eta) + 6\eta^2 log\eta^3 f'(\eta) + 18\eta^2 log\eta^4 f'(\eta)$$

$$+7\eta^2 log\eta^5 f'(\eta) + 6\eta log\eta^3 f(\eta) + 6\eta log\eta^4 f(\eta) + \eta log\eta^5 f(\eta) + \eta^2 log\eta Ha^2 f'(\eta) +$$

$$\eta log\eta Ha^2 f(\eta) + Re\lambda_\theta = 0 \qquad (4)$$

Boundary conditions being: $\frac{1}{r}\frac{\partial\psi}{\partial\theta} = f'(\eta) = f(\eta) = 0$ on Γ

3.2 Finite Element Method (FEM)

In Finite Element Method (FEM), Reddy [6], the solution has E elements and $N = E + 1$ nodes. The approximate solution is C^0 continuous, i.e only the 0^{th} order solution is continuous across element interfaces.

3.2.1 Method of weighted residuals

Equation (4) is the strong form of the problem. It's weak form is obtained using method of weighted residual and is given by

$$\begin{aligned}
&\int_{\Omega}\left[2\eta^2 log\eta^3 w(\eta)f'(\eta)+5\eta^2 log\eta^4 w(\eta)f'(\eta)+\eta^2 log\eta^5 w(\eta)f'(\eta)\right]d\eta\\
&+\int_{\Omega}\left[4\eta^3 log\eta^4 w'(\eta)f'(\eta)+2\eta^3 log\eta^5 w'(\eta)f'(\eta)+6\eta log\eta^3 w(\eta)f(\eta)\right]d\eta\\
&+\int_{\Omega}\left[6\eta log\eta^4 w(\eta)f(\eta)+\eta log\eta^5 w(\eta)f(\eta)+\eta^2 log\eta Ha^2 w(\eta)f'(\eta)\right]d\eta\\
&+\int_{\Omega}\left[\eta log\eta Ha^2 w(\eta)f(\eta)+w(\eta)Re\lambda_\theta\right]d\eta=-\int_{\Gamma}\eta^4 log\eta^5 w(\eta)f''(\eta)n_\eta d\Gamma\\
&-\int_{\Gamma}\eta^3 log\eta^4 w(\eta)f'(\eta)n_\eta d\Gamma+\int_{\Gamma}\eta^4 log\eta^5 w'(\eta)f'(\eta)n_\eta d\Gamma-\int_{\Gamma}2\eta^3 log\eta^5 w(\eta)f'(\eta)n_\eta d\Gamma
\end{aligned} \tag{5}$$

Where n_η is the η component of unit outward normal of boundary. n_η is equal to -1 and 1 at the left and right boundaries of the problem domain respectively. The terms on the right of equation (5) provide the boundary conditions. For velocity, these values are zero considering no-slip condition.

3.2.2 Approximate solution using shape functions and Galerkin Method

On letting approximate solution as $f_{app}(\eta)=\sum_{j=1}^{N} f_j s_j(\eta)$, where f_{app} is the approximate solution to be found, N is the number of nodes in the finite element mesh, f_j's are the nodal unknown values that will be calculated at the end of finite element solution and s_j's are the shape (basis) functions that are used to construct the approximate solution. The shape functions have compact support and possess Kronecker-delta property . In the Galerkin Method, weight functions of equation (5) are set such that $w(\eta)=s_i(\eta)$. Putting $f_{app}(\eta)=\sum_{j=1}^{N} f_j s_j(\eta)$ and $w(\eta)=s_i(\eta)$ in equation (5), it changes to

$$\begin{aligned}
&\sum_{j=1}^{N}\left[\int_{\Omega}\left\{2\eta^2 log\eta^3 s_i(\eta)s_j'(\eta)+5\eta^2 log\eta^4 s_i(\eta)s_j'(\eta)+\eta^2 log\eta^5 s_i(\eta)s_j'(\eta)\right\}d\eta\right]f_j\\
&+\sum_{j=1}^{N}\left[\int_{\Omega}\left\{4\eta^3 log\eta^4 s_i'(\eta)s_j'(\eta)+2\eta^3 log\eta^5 s_i'(\eta)s_j'(\eta)+6\eta log\eta^3 s_i(\eta)s_j(\eta)\right\}d\eta\right]f_j\\
&+\sum_{j=1}^{N}\left[\int_{\Omega}\left\{6\eta log\eta^4 s_i(\eta)s_j(\eta)+\eta log\eta^5 s_i(\eta)s_j(\eta)+\eta^2 log\eta Ha^2 s_i(\eta)s_j'(\eta)\right\}d\eta\right]f_j
\end{aligned}$$

$$+\sum_{j=1}^{N}\left[\int_{\Omega}\left\{\eta log\eta Ha^{2}s_{i}(\eta)s_{j}(\eta)\right\}d\eta\right]f_{j}=-\int_{\Omega}s_{i}(\eta)Re\lambda_{\theta}d\eta \qquad i=1,2,...,N \tag{6}$$

3.2.3 Global equation and elemental systems

Equation (6) is expressed in global equation system matrix notation by $[W]\{X\}=\{Y\}$, where $[W]$ is the square stiffness matrix of size $N\times N$, $\{X\}$ is the vector of nodal unknowns with N entries. $\{Y\}$ is the global force vector of size $N\times 1$. From equation (6)

$$W_{ij}=\sum_{j=1}^{N}\left[\int_{\Omega}\left\{2\eta^{2}log\eta^{3}s_{i}(\eta)s_{j}'(\eta)+5\eta^{2}log\eta^{4}s_{i}(\eta)s_{j}'(\eta)+\eta^{2}log\eta^{5}s_{i}(\eta)s_{j}'(\eta)\right\}d\eta\right]f_{j}$$

$$+\sum_{j=1}^{N}\left[\int_{\Omega}\left\{4\eta^{3}log\eta^{4}s_{i}'(\eta)s_{j}'(\eta)+2\eta^{3}log\eta^{5}s_{i}'(\eta)s_{j}'(\eta)+6\eta log\eta^{3}s_{i}(\eta)s_{j}(\eta)\right\}d\eta\right]f_{j}$$

$$+\sum_{j=1}^{N}\left[\int_{\Omega}\left\{6\eta log\eta^{4}s_{i}(\eta)s_{j}(\eta)+\eta log\eta^{5}s_{i}(\eta)s_{j}(\eta)+\eta^{2}log\eta Ha^{2}s_{i}(\eta)s_{j}'(\eta)\right\}d\eta\right]f_{j}$$

$$+\sum_{j=1}^{N}\left[\int_{\Omega}\left\{\eta log\eta Ha^{2}s_{i}(\eta)s_{j}(\eta)\right\}d\eta\right]f_{j},\quad X_{j}=f_{j}\quad \text{and}\quad Y_{i}=-\int_{\Omega}s_{i}(\eta)Re\lambda_{\theta}d\eta \tag{7}$$

From equation (7), the expression for W_{ij} provides the elemental stiffness matrix, W_{ij}^{e}, which is obtained by neglecting the summation sign and f_j.

3.2.4 Gauss quadrature integration

To evaluate W_{ij}^{e} integral using Gauss quadrature limits of W_{ij}^{e} integral are $\eta=\eta_{1}^{e}$ and $\eta=\eta_{2}^{e}$ which are the coordinates of the two end points of the element. Limits of the integral are changed to be -1 and 1 which require change of variable. This leads to the use of master element in evaluating elemental integrals. Using the Kroncker-delta property of shape functions, they are written in terms of the master element coordinate ξ as

$$s_{1}=\frac{1}{2}(1-\xi)\ \text{and}\ s_{2}=\frac{1}{2}(1+\xi) \tag{8}$$

To evaluate W_{ij}^{e} integrals, the global η coordinate is related to ξ coordinate by

$$\eta=\frac{h^{e}}{2}\xi+\frac{\eta_{1}^{e}+\eta_{2}^{e}}{2} \tag{9}$$

where h^e is the length of element, e, given by $h^e = \eta_2^e - \eta_1^e$. W_{ij}^e is written using the ξ coordinate and new limits for Gauss quadrature integration and upon defining Finite Element Jacobian as $J^e = \frac{d\eta}{d\xi} = \frac{h^e}{2}$, transforms to

$$W_{ij}^e = \int_{-1}^{1} \left\{ 2\eta^2 log\eta^3 s_i \frac{ds_j}{d\xi} + 5\eta^2 log\eta^4 s_i \frac{ds_j}{d\xi} + \eta^2 log\eta^5 s_i \frac{ds_j}{d\xi} + 4\eta^3 log\eta^4 \frac{ds_i}{d\xi}\frac{ds_j}{d\xi}\frac{1}{J^e} \right\} d\xi$$

$$+ \int_{-1}^{1} \left\{ 2\eta^3 log\eta^5 \frac{ds_i}{d\xi}\frac{ds_j}{d\xi}\frac{1}{J^e} + 6\eta log\eta^3 s_i s_j J^e + 6\eta log\eta^4 s_i s_j J^e + \eta log\eta^5 s_i s_j J^e \right\} d\xi$$

$$+ \int_{-1}^{1} \left\{ \eta^2 log\eta Ha^2 s_i \frac{ds_j}{d\xi} + \eta log\eta Ha^2 s_i s_j J^e \right\} d\xi \qquad (10)$$

3.2.5 Assembly process

Elemental stiffness matrices are assembled in global system of equation e.g for a mesh of 5 linear elements with global node numbers, local to global node mapping matrix results in the following global equation system for 6 node mesh

$$\begin{bmatrix} W_{11}^1 & W_{12}^1 & 0 & 0 & 0 & 0 \\ W_{21}^1 & W_{22}^1 + W_{11}^2 & W_{12}^2 & 0 & 0 & 0 \\ 0 & W_{21}^2 & W_{22}^2 + W_{11}^3 & W_{12}^3 & 0 & 0 \\ 0 & 0 & W_{21}^3 & W_{22}^3 + W_{11}^4 & W_{12}^4 & 0 \\ 0 & 0 & 0 & W_{21}^4 & W_{22}^4 + W_{11}^5 & W_{12}^5 \\ 0 & 0 & 0 & 0 & W_{21}^5 & W_{22}^5 + W_{11}^6 \end{bmatrix} \begin{Bmatrix} f_1 \\ f_2 \\ f_3 \\ f_4 \\ f_5 \\ f_6 \end{Bmatrix}$$

$$= \begin{Bmatrix} Y_1^1 \\ Y_2^1 + Y_1^2 \\ Y_2^2 + Y_1^3 \\ Y_2^3 + Y_1^4 \\ Y_2^4 + Y_1^5 \\ Y_2^5 \end{Bmatrix} \qquad (11)$$

Elemental force vector components are evaluated using equation (7) and placed in equation (11). The resulting equation is trimmed and hands out

$$\begin{bmatrix} W_{22}^1 + W_{11}^2 & W_{12}^2 & 0 & 0 \\ W_{21}^2 & W_{22}^2 + W_{11}^3 & W_{12}^3 & 0 \\ 0 & W_{21}^3 & W_{22}^3 + W_{11}^4 & W_{12}^4 \\ 0 & 0 & W_{21}^4 & W_{22}^4 + W_{11}^5 \end{bmatrix} \begin{Bmatrix} f_2 \\ f_3 \\ f_4 \\ f_5 \end{Bmatrix} = \begin{Bmatrix} -2Re\lambda_\theta \\ \vdots \\ \vdots \end{Bmatrix} \qquad (12)$$

3.2.6 Discretization of major axis of elliptical cross section of pipe

The major axis of the elliptical cross section of the pipe is sub divided into N-1 elements and N nodes as shown in figure 2.

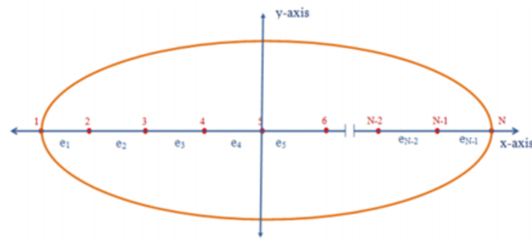

Figure 2: Discretized major axis of elliptical cross section of pipe

3.2.7 Calculation of elemental stiffness matrix

Elemental stiffness matrix is evaluated using equations (8), (9) and (10) such that: Setting $h^e = 0.0002, \eta_1^e = 0.0000$ and $\eta_2^e = 0.0002$ then $\eta = 0.0001\xi + 0.0001$ so that equation (10) produces

$$W_{11}^1 = 1.02009\times10^{-4}+2.03417\times10^{-7}Ha^2-2.99146\times10^{-2}Ha^2J^e-\frac{8.07356\times10^{-8}}{J^e} -1.28685J^e \tag{13}$$

$$W_{12}^1 = -1.02009\times10^{-4}-2.03417\times10^{-8}Ha^2-2.52849\times10^{-2}Ha^2J^e+\frac{8.07356\times10^{-8}}{J^e} -0.889363J^e \tag{14}$$

$$W_{21}^1 = -2.39048\times10^{-4}+8.76719\times10^{-8}Ha^2-2.52849\times10^{-2}Ha^2J^e+\frac{8.07352\times10^{-8}}{J^e} -0.889363J^e \tag{15}$$

$$W_{22}^1 = -2.39052\times10^{-4}-8.17592\times10^{-8}Ha^2-6.75332\times10^{-2}Ha^2J^e-\frac{8.07356\times10^{-8}}{J^e} -2.0668J^e \tag{16}$$

The 2×2 $[W^e]$ elemental matrix is given by

$$W^e = \begin{bmatrix} W_{11}^1 & W_{12}^1 \\ W_{21}^1 & W_{22}^1 \end{bmatrix} \tag{17}$$

From now henceforth, when equation (17) is mentioned, it means it comprises equations (13) to (16) which are too large to fit in the matrix.

4 Results

4.1 Varying Hartmann number

Values of Hartmann number engaged are 1.0, 5.0 and 10.0, while $J^e = 0.0001$, $\lambda_\theta = 0.001$, $Re = 1.0$, and $a = 0.0034$. When values of Ha and J^e are put in equation (17) an elemental matrix, W^e is formed. W^e is employed to produce stiffness matrix W. Considering 35 nodes in figure 2, substituting W, Re and λ_θ in equation (12), a system of algebraic equations is formed. The equations are solved by manupulating Mathematica which provides solutions of f_j's as f_j^1's for $Ha = 1.0$, f_j^2's for $Ha = 5.0$ and f_j^3's for $Ha = 10.0$ in table 1. f_j's are the velocities of fluid along the major axis of cross section of elliptical pipe.

Table 1: Velocities along the major axis when $Ha = 1.0, 5.0, 10.0$

$f_1^1 = 0.000$	$f_2^1 = 0.869$	$f_3^1 = 1.340$	$f_4^1 = 1.594$	$f_5^1 = 1.732$	$f_6^1 = 1.807$	$f_7^1 = 1.847$
$f_1^2 = 0.000$	$f_2^2 = 0.650$	$f_3^2 = 0.929$	$f_4^2 = 1.048$	$f_5^2 = 1.100$	$f_6^2 = 1.122$	$f_7^2 = 1.131$
$f_1^3 = 0.000$	$f_2^3 = 0.384$	$f_3^3 = 0.477$	$f_4^3 = 0.499$	$f_5^3 = 0.505$	$f_6^3 = 0.506$	$f_7^3 = 0.506$
$f_8^1 = 1.869$	$f_9^1 = 1.881$	$f_{10}^1 = 1.887$	$f_{11}^1 = 1.891$	$f_{12}^1 = 1.892$	$f_{13}^1 = 1.893$	$f_{14}^1 = 1.894$
$f_8^2 = 1.135$	$f_9^2 = 1.137$	$f_{10}^2 = 1.138$	$f_{11}^2 = 1.138$	$f_{12}^2 = 1.138$	$f_{13}^2 = 1.138$	$f_{14}^2 = 1.138$
$f_8^3 = 0.506$	$f_9^3 = 0.506$	$f_{10}^3 = 0.506$	$f_{11}^3 = 0.506$	$f_{12}^3 = 0.506$	$f_{13}^3 = 0.506$	$f_{14}^3 = 0.506$
$f_{15}^1 = 1.894$	$f_{16}^1 = 1.894$	$f_{17}^1 = 1.895$	$f_{18}^1 = 1.895$	$f_{19}^1 = 1.895$	$f_{20}^1 = 1.895$	$f_{21}^1 = 1.895$
$f_{15}^2 = 1.138$	$f_{16}^2 = 1.138$	$f_{17}^2 = 1.732$	$f_{18}^2 = 1.807$	$f_{19}^2 = 1.138$	$f_{20}^2 = 1.138$	$f_{21}^2 = 1.138$
$f_{15}^3 = 0.506$	$f_{16}^3 = 0.506$	$f_{17}^3 = 0.506$	$f_{18}^3 = 0.506$	$f_{19}^3 = 0.506$	$f_{20}^3 = 0.506$	$f_{21}^3 = 0.506$
$f_{22}^1 = 1.895$	$f_{23}^1 = 1.895$	$f_{24}^1 = 1.895$	$f_{25}^1 = 1.895$	$f_{26}^1 = 1.895$	$f_{27}^1 = 1.894$	$f_{28}^1 = 1.893$
$f_{22}^2 = 1.138$	$f_{23}^2 = 1.138$	$f_{24}^2 = 1.138$	$f_{25}^2 = 1.138$	$f_{26}^2 = 1.138$	$f_{27}^2 = 1.138$	$f_{28}^2 = 1.138$
$f_{22}^3 = 0.506$	$f_{23}^3 = 0.506$	$f_{24}^3 = 0.506$	$f_{25}^3 = 0.506$	$f_{26}^3 = 0.506$	$f_{27}^3 = 0.506$	$f_{28}^3 = 0.506$
$f_{29}^1 = 1.891$	$f_{30}^1 = 1.885$	$f_{31}^1 = 1.867$	$f_{32}^1 = 1.815$	$f_{33}^1 = 1.665$	$f_{34}^1 = 1.235$	$f_{35}^1 = 0.000$
$f_{29}^2 = 1.138$	$f_{30}^2 = 1.137$	$f_{31}^2 = 1.133$	$f_{32}^2 = 1.117$	$f_{33}^2 = 1.059$	$f_{34}^2 = 0.837$	$f_{35}^2 = 0.000$
$f_{29}^3 = 0.506$	$f_{30}^3 = 0.506$	$f_{31}^3 = 0.506$	$f_{32}^3 = 0.506$	$f_{33}^3 = 0.499$	$f_{34}^3 = 0.445$	$f_{35}^3 = 0.000$

Incorporating velocities in table 1 and plotting velocity against nodes which are points on the major axis of the pipe, delivers the form in figure 3.

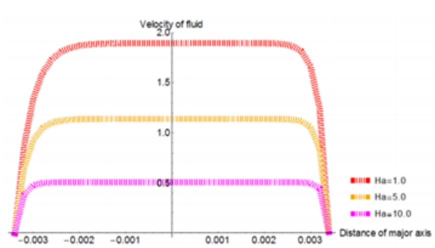

Figure 3: Combined velocity profiles for $Ha = 1.0$, $Ha = 5.0$ and $Ha = 10.0$

4.2 Altering gravitational force

Gravitational force values embraced are 0.00002, 0.00004 and 0.00008 when $J^e = 0.0001, Ha = 1.0, Re = 1.0$, and $a = 0.0034$. Using the same method in §4.1 by applying above mentioned values, Mathematica conveys solutions in table 2

Table 2: Velocities along the major axis for $\lambda_\theta = 0.00002, 0.00004, 0.00008$

$f_1^1 = 0.000$	$f_2^1 = 0.017$	$f_3^1 = 0.027$	$f_4^1 = 0.032$	$f_5^1 = 0.036$	$f_6^1 = 0.036$	$f_7^1 = 0.037$
$f_1^2 = 0.000$	$f_2^2 = 0.034$	$f_3^2 = 0.054$	$f_4^2 = 0.064$	$f_5^2 = 0.069$	$f_6^2 = 0.072$	$f_7^2 = 0.074$
$f_1^3 = 0.000$	$f_2^3 = 0.069$	$f_3^3 = 0.107$	$f_4^3 = 0.128$	$f_5^3 = 0.139$	$f_6^3 = 0.145$	$f_7^3 = 0.145$
$f_8^1 = 0.038$	$f_9^1 = 0.038$	$f_{10}^1 = 0.038$	$f_{11}^1 = 0.038$	$f_{12}^1 = 0.038$	$f_{13}^1 = 0.038$	$f_{14}^1 = 0.038$
$f_8^2 = 0.075$	$f_9^2 = 0.075$	$f_{10}^2 = 0.075$	$f_{11}^2 = 0.076$	$f_{12}^2 = 0.076$	$f_{13}^2 = 0.076$	$f_{14}^2 = 0.076$
$f_8^3 = 0.150$	$f_9^3 = 0.150$	$f_{10}^3 = 0.151$	$f_{11}^3 = 0.151$	$f_{12}^3 = 0.151$	$f_{13}^3 = 0.151$	$f_{14}^3 = 0.151$
$f_{15}^1 = 0.038$	$f_{16}^1 = 0.038$	$f_{17}^1 = 0.038$	$f_{18}^1 = 0.038$	$f_{19}^1 = 0.038$	$f_{20}^1 = 0.038$	$f_{21}^1 = 0.038$
$f_{15}^2 = 0.076$	$f_{16}^2 = 0.076$	$f_{17}^2 = 0.076$	$f_{18}^2 = 0.076$	$f_{19}^2 = 0.076$	$f_{20}^2 = 0.076$	$f_{21}^2 = 0.076$
$f_{15}^3 = 0.151$	$f_{16}^3 = 0.151$	$f_{17}^3 = 0.151$	$f_{18}^3 = 0.151$	$f_{19}^3 = 0.151$	$f_{20}^3 = 0.151$	$f_{21}^3 = 0.151$
$f_{22}^1 = 0.038$	$f_{23}^1 = 0.038$	$f_{24}^1 = 0.038$	$f_{25}^1 = 0.038$	$f_{26}^1 = 0.038$	$f_{27}^1 = 0.038$	$f_{28}^1 = 0.038$
$f_{22}^2 = 0.076$	$f_{23}^2 = 0.076$	$f_{24}^2 = 0.076$	$f_{25}^2 = 0.076$	$f_{26}^2 = 0.076$	$f_{27}^2 = 0.076$	$f_{28}^2 = 0.076$
$f_{22}^3 = 0.151$	$f_{23}^3 = 0.151$	$f_{24}^3 = 0.151$	$f_{25}^3 = 0.151$	$f_{26}^3 = 0.151$	$f_{27}^3 = 0.151$	$f_{28}^3 = 0.151$
$f_{29}^1 = 0.038$	$f_{30}^1 = 0.038$	$f_{31}^1 = 0.037$	$f_{32}^1 = 0.036$	$f_{33}^1 = 0.033$	$f_{34}^1 = 0.025$	$f_{35}^1 = 0.000$
$f_{29}^2 = 0.076$	$f_{30}^2 = 0.076$	$f_{31}^2 = 0.075$	$f_{32}^2 = 0.073$	$f_{33}^2 = 0.067$	$f_{34}^2 = 0.049$	$f_{35}^2 = 0.000$
$f_{29}^3 = 0.151$	$f_{30}^3 = 0.151$	$f_{31}^3 = 0.149$	$f_{32}^3 = 0.145$	$f_{33}^3 = 0.133$	$f_{34}^3 = 0.099$	$f_{35}^3 = 0.000$

Constructing on the same axis velocities in tables 2 against distance of major axis gives figure 4.

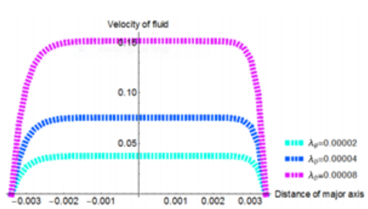

Figure 4: Combined velocity profiles for $\lambda_\theta = 0.00002, \lambda_\theta = 0.00004$ and $\lambda_\theta = 0.0000$

4.3 Modifying Reynolds number

Reynolds number values employed are 2.0, 4.0 and 8.0 while $J^e = 0.0001, \lambda_\theta = 0.001, Ha = 1.0$, and $a = 0.0034$. Following the same steps as in §4.1 and engaging criterion above furnishes velocities in table 3.

Table 3: Velocities along the major axis with $Re = 2.0, 4.0, 8.0$

$f_1^1 = 0.000$	$f_2^1 = 1.738$	$f_3^1 = 2.679$	$f_4^1 = 3.188$	$f_5^1 = 3.464$	$f_6^1 = 3.613$	$f_7^1 = 3.694$
$f_1^2 = 0.000$	$f_2^2 = 3.477$	$f_3^2 = 5.358$	$f_4^2 = 6.377$	$f_5^2 = 6.928$	$f_6^2 = 7.227$	$f_7^2 = 7.399$
$f_1^3 = 0.000$	$f_2^3 = 6.95$	$f_3^3 = 10.72$	$f_4^3 = 12.75$	$f_5^3 = 13.86$	$f_6^3 = 14.45$	$f_7^3 = 14.78$
$f_8^1 = 3.738$	$f_9^1 = 3.761$	$f_{10}^1 = 3.774$	$f_{11}^1 = 3.781$	$f_{12}^1 = 3.785$	$f_{13}^1 = 3.787$	$f_{14}^1 = 3.788$
$f_8^2 = 7.476$	$f_9^2 = 7.523$	$f_{10}^2 = 7.548$	$f_{11}^2 = 7.562$	$f_{12}^2 = 7.570$	$f_{13}^2 = 7.574$	$f_{14}^2 = 7.576$
$f_8^3 = 14.95$	$f_9^3 = 15.01$	$f_{10}^3 = 15.10$	$f_{11}^3 = 15.13$	$f_{12}^3 = 15.14$	$f_{13}^3 = 15.15$	$f_{14}^3 = 15.15$
$f_{15}^1 = 3.789$	$f_{16}^1 = 3.789$	$f_{17}^1 = 3.789$	$f_{18}^1 = 3.789$	$f_{19}^1 = 3.789$	$f_{20}^1 = 3.789$	$f_{21}^1 = 3.789$
$f_{15}^2 = 7.577$	$f_{16}^2 = 7.578$	$f_{17}^2 = 7.578$	$f_{18}^2 = 7.578$	$f_{19}^2 = 7.579$	$f_{20}^2 = 7.579$	$f_{21}^2 = 7.579$
$f_{15}^3 = 15.15$	$f_{16}^3 = 15.16$	$f_{17}^3 = 15.16$	$f_{18}^3 = 15.16$	$f_{19}^3 = 15.16$	$f_{20}^3 = 15.16$	$f_{21}^3 = 15.16$
$f_{22}^1 = 3.789$	$f_{23}^1 = 3.789$	$f_{24}^1 = 3.789$	$f_{25}^1 = 3.789$	$f_{26}^1 = 3.789$	$f_{27}^1 = 3.789$	$f_{28}^1 = 3.787$
$f_{22}^2 = 7.579$	$f_{23}^2 = 7.579$	$f_{24}^2 = 7.579$	$f_{25}^2 = 7.578$	$f_{26}^2 = 7.578$	$f_{27}^2 = 7.577$	$f_{28}^2 = 7.574$
$f_{22}^3 = 15.16$	$f_{23}^3 = 15.16$	$f_{24}^3 = 15.16$	$f_{25}^3 = 15.16$	$f_{26}^3 = 15.16$	$f_{27}^3 = 15.15$	$f_{28}^3 = 15.15$
$f_{29}^1 = 3.783$	$f_{30}^1 = 3.770$	$f_{31}^1 = 3.733$	$f_{32}^1 = 3.630$	$f_{33}^1 = 3.331$	$f_{34}^1 = 2.471$	$f_{35}^1 = 0.000$
$f_{29}^2 = 7.565$	$f_{30}^2 = 7.540$	$f_{31}^2 = 7.468$	$f_{32}^2 = 7.259$	$f_{33}^2 = 6.661$	$f_{34}^2 = 4.942$	$f_{35}^2 = 0.000$
$f_{29}^3 = 15.13$	$f_{30}^3 = 15.08$	$f_{31}^3 = 14.94$	$f_{32}^3 = 14.52$	$f_{33}^3 = 13.32$	$f_{34}^3 = 9.884$	$f_{35}^3 = 0.000$

Bringing together velocities in tables 3 on the same axis supplies figuration in figure 5.

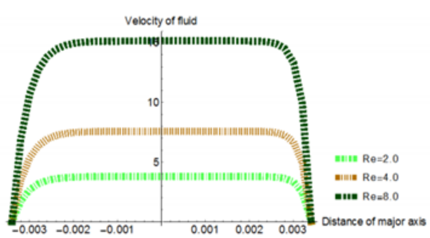

Figure 5: Combined velocity contours for $Re = 2.0, Re = 4.0$ and $Re = 8.0$

4.4 Changing distance of half major axis

Values of half major axis adopted are 0.0020, 0.0028 and 0.0032 when $J^e = 0.0001, \lambda_\theta = 0.025, Ha = 1.0$, and $Re = 1.0$. Repeating the steps in §4.1 utilizing aforementioned values presents solutions in table 4.

Table 4: Velocities along the major axis when $a = 0.0020, 0.0028, 0.0032$

$f_1^1 = 0.000$	$f_2^1 = 21.73$	$f_3^1 = 33.49$	$f_4^1 = 39.86$	$f_5^1 = 43.30$	$f_6^1 = 45.17$	$f_7^1 = 46.18$
$f_1^2 = 0.000$	$f_2^2 = 21.73$	$f_3^2 = 33.49$	$f_4^2 = 39.86$	$f_5^2 = 43.30$	$f_6^2 = 45.17$	$f_7^2 = 46.18$
$f_1^3 = 0.000$	$f_2^3 = 21.73$	$f_3^3 = 33.49$	$f_4^3 = 39.86$	$f_5^3 = 43.30$	$f_6^3 = 45.17$	$f_7^3 = 46.18$
$f_8^1 = 46.72$	$f_9^1 = 47.02$	$f_{10}^1 = 47.18$	$f_{11}^1 = 47.26$	$f_{12}^1 = 47.30$	$f_{13}^1 = 47.33$	$f_{14}^1 = 47.32$
$f_8^2 = 46.72$	$f_9^2 = 47.02$	$f_{10}^2 = 47.18$	$f_{11}^2 = 47.26$	$f_{12}^2 = 47.31$	$f_{13}^2 = 47.34$	$f_{14}^2 = 47.35$
$f_8^3 = 46.72$	$f_9^3 = 47.02$	$f_{10}^3 = 47.18$	$f_{11}^3 = 47.26$	$f_{12}^3 = 47.31$	$f_{13}^3 = 47.34$	$f_{14}^3 = 47.35$
$f_{15}^1 = 47.27$	$f_{16}^1 = 47.12$	$f_{17}^1 = 46.67$	$f_{18}^1 = 45.37$	$f_{19}^1 = 41.63$	$f_{20}^1 = 30.89$	$f_{21}^1 = 0.000$
$f_{15}^2 = 47.36$	$f_{16}^2 = 47.36$	$f_{17}^2 = 47.36$	$f_{18}^2 = 47.37$	$f_{19}^2 = 47.36$	$f_{20}^2 = 47.36$	$f_{21}^2 = 47.36$
$f_{15}^3 = 47.36$	$f_{16}^3 = 47.362$	$f_{17}^3 = 47.36$	$f_{18}^3 = 47.37$	$f_{19}^3 = 47.37$	$f_{20}^3 = 47.37$	$f_{21}^3 = 47.37$
$f_{22}^2 = 47.33$	$f_{23}^2 = 47.28$	$f_{24}^2 = 47.13$	$f_{25}^2 = 46.67$	$f_{26}^2 = 45.37$	$f_{27}^2 = 41.63$	$f_{28}^2 = 30.89$
$f_{22}^3 = 47.37$	$f_{23}^3 = 47.37$	$f_{24}^3 = 47.36$	$f_{25}^3 = 47.36$	$f_{26}^3 = 47.34$	$f_{27}^3 = 47.28$	$f_{28}^3 = 47.13$
$f_{29}^2 = 0.000$						
$f_{29}^3 = 46.67$	$f_{30}^3 = 45.37$	$f_{31}^3 = 41.63$	$f_{32}^3 = 30.89$	$f_{33}^3 = 0.000$		

Drawing together velocities in tables 4 against distance of major axis procures the sketch in figure 6.

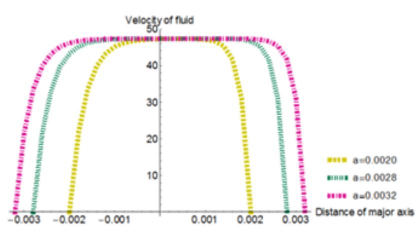

Figure 6: Combined velocity forms for $a = 0.0020, a = 0.0028$ and $a = 0.0032$

5 Conclusion

Velocity figuration for MHD flow in a straight horizontal pipe of elliptical cross section has been described after formulation and numerical solution of governing equations. The outcomes reveal that: When Hartmann number is increased, velocity decreases at the centre of pipe, figure 3. Hike in gravitational force, Reynolds number and distance of half major axis results in rise in fluid velocity at the centre of pipe, figures 4 to 6, though, the spike is small for the last situation. Velocity distribution shrinks from the centre of the pipe to the edges where it is zero in all the four situations.

References

[1] C. Muhim and N. Deka, Numerical Solution of MHD Flow in an Insulated Rectangular Duct under the Action of Strong Transverse Magnetic Field by Finite Difference Method, *International Journal of Energy and Technology*, **6** (10) (2014), 1-8.

[2] D. Abbott, H. Arthur and Tsung-Yen, Similarity Analyses of Partial Differential Equations, ORA project, The University of Michigan, (1967), 1-130.

[3] V. C. Loukopoulos, G. C. Bourantas, E. D. Skouras, G. C. Nikiforidis, Localised Meshless Point Collocation Method for Time Dependent Magnetohydrodynamic Flow Through Pipes under a Variety of Wall Conductivities, *Comput. Mech.*, **47** (2011), 137-159. https://doi.org/10.1007/s00466-010-0535-8

[4] K. Josef, *Dimensionless Physical Quantities in Science and Engineering*, Elsevier, London, 2012. https://doi.org/10.1016/c2011-0-06212-9

[5] M. Prasanna and S. Ganesh, Magnetohydrodynamic Flow Through Ducts with Different Cross Section, *International Journal of Recent Technology and Engineering*, **8** (2019), issue 3S2, 853-859.
https://doi.org/10.35940/ijrte.c1259.1083s219

[6] N. Reddy, *Introduction to the Finite Element Method* , McGraw-Hill Education, New York, 2019.

Received: April 27, 2021; Published: May 27, 2021